The Astrophysical Journal, 664:L5–L8, 2007 July 20

OBSERVATIONS OF THE OPTICAL AFTERGLOW OF GRB 050319: THE WIND-TO-ISM TRANSITION IN VIEW

Atish Kamble,[1] L. Resmi,[1,2] and Kuntal Misra[3]

Received 2007 February 5; accepted 2007 May 31; published 2007 June 28

ABSTRACT

The collapse of a massive star is believed to be the most probable progenitor of a long gamma-ray burst (GRB). Such a star is expected to have its environment modified by the stellar wind. The effect of such a circumstellar wind medium is expected to be seen in the evolution of a GRB afterglow, but so far this has not been conclusively found. We claim that a signature of the transition from wind to constant density medium of the circumburst medium is visible in the afterglow of GRB 050319. Along with the optical observations of the afterglow of GRB 050319, we present a model for the multiband afterglow of GRB 050319. We show that the break seen in the optical light curve at ~0.02 days could be explained as being due to the transition from wind to constant density medium of the circumburst medium, in which case, to our knowledge, this could be the first ever detection of such a transition at any given frequency band. Detection of such a transition could also serve as confirmation of the massive star collapse scenario for GRB progenitors, independent of supernova signatures.

Subject heading: gamma rays: bursts

1. INTRODUCTION

One of the long-standing questions in astrophysics is what the progenitors of gamma-ray bursts (GRBs) are. A massive star that has collapsed is one of the most favored progenitors of long GRBs. Evidence of a massive star being a GRB progenitor may be obtained in two different ways, both using observations of GRB afterglows:

1. *A supernova component underlying the GRB afterglow*.—A few of the nearby GRB afterglows have shown the temporal and spectroscopic signature of an underlying supernova (see, e.g., Stanek et al. 2003).
2. *Evolution of GRB afterglow in the stellar wind medium*.—Massive stars modify the density profile of the circumstellar medium due to the powerful winds that they drive during their lifetime. For a constant mass-loss rate and a constant wind velocity, the circumburst medium assumes a density profile $\rho \propto r^{-2}$ as compared to $\rho =$ constant in the absence of stellar wind.

The evolution of the GRB afterglow light curves is significantly different in these two cases of density profiles (Wijers & Galama 1999; Chevalier & Li 2000). Attempts to look for the signatures of such a wind-modified circumburst density profile in the light curves of GRB afterglows have not been conclusive so far. In the case of GRB 050904, Gendre et al. (2007) find that the early X-ray afterglow suggests a windlike density profile of the circumburst medium, while the late optical afterglow was consistent with evolution in a constant density medium. Hence, they conjecture that a transition between these two types of density profiles would have taken place somewhere in between. However, this transition was not directly observed in the light curve of any given band. We show that the afterglow of GRB 050319 could be explained as being due to the transition of the circumburst density profile from a windlike denisty to a constant density.

GRB 050319 was detected by the Burst Alert Telescope (BAT) on the *Swift* satellite on 2005 March 19, 09:31:18.44 UT (Krimm et al. 2005a, 2005b). However, Cusumano et al. (2006), using the reanalysis of the BAT data, pointed out that *Swift* was slewing during the GRB onset and that the BAT trigger was switched off. The GRB was recognized about 135 s after its actual onset. The total duration of the GRB (T_{90}) was thus 149.7 s (Cusumano et al. 2006) instead of 10 ± 2 s (Krimm et al. 2005a, 2005b). The burst fluence in the 15–350 keV band within the T_{90} duration is estimated to be 1.6×10^{-6} ergs cm^{-2}. The photon index of the time-averaged single–power-law spectrum is 2.1 ± 0.2. The *Swift* XRT and UV/Optical Telescope (UVOT) located a bright source at $\alpha = 10^{h}16^{m}48^{s}$, $\delta = +43°32'47''$ (J2000) that was later confirmed by Rykoff et al. (2005) with ROTSE-IIIb. Fynbo et al. (2005) obtained the spectra of the afterglow of GRB 050319 on 2005 March 20, and the redshift of the afterglow was measured to be $z = 3.24$. At this redshift, the gamma-ray isotropic equivalent energy released during the burst was 3.7×10^{52} ergs for a flat universe with $\Omega_m = 0.3$, $\Omega_\Lambda = 0.7$, and $H_0 = 70$ km s^{-1} Mpc^{-1}.

2. OBSERVATIONS AND DATA REDUCTION

Optical CCD observations of the afterglow of GRB 050319 were carried out in Johnson *BV* and Cousins *RI* filters using the 104 cm Sampurnanand Telescope of ARIES, Nainital, India, with regular specifications of the CCD camera and using standard observation procedures of bias subtraction and flat-fielding. For details, see Misra et al. (2007).

The *BVRI* magnitudes of the optical transient obtained were calibrated differentially using secondary stars numbered 8, 9, 10, 11, and 13 in the list of Henden (2005). The magnitudes derived in this way are given in Table 1. The photometric magnitudes that are available in the literature by Woźniak et al. (2005), Quimby et al. (2006), Mason et al. (2006), and Huang et al. (2007) were converted to the present photometric scales using the five secondary stars mentioned above.

3. LIGHT CURVES OF GRB 050319

Along with our own observations, we have used the observations reported in the literature to study the light curves of the GRB 050319 afterglow. The X-ray afterglow was observed by *Swift* XRT starting from ~220 s to 28 days (Cusumano et

[1] Raman Research Institute, Bangalore 560-080, India.
[2] Joint Astronomy Programme, Indian Institute of Science, Bangalore 560-012, India.
[3] Aryabhatta Research Institute of Observational Sciences, Manora Peak, Nainital 263-129, India.

TABLE 1
CCD *BVRI* Broadband Optical Observations of the GRB 050319 Afterglow

Date (UT) 2005 March	Magnitude	Exposure Time (s)	Passband
19.7512	21.02 ± 0.14	2 × 900	*B*
19.7457	20.23 ± 0.20	600	*V*
19.8558	20.60 ± 0.21	600	*V*
19.6949	19.46 ± 0.16	300	*R*
19.6999	19.25 ± 0.10	300	*R*
19.7215	19.98 ± 0.11	300	*R*
19.7539	20.06 ± 0.13	300	*R*
19.7874	20.03 ± 0.16	300	*R*
19.7129	19.59 ± 0.19	300	*I*
19.7587	19.66 ± 0.25	300	*I*

Note.—Using the 104 cm Sampurnanand Telescope at ARIES, Nainital, India.

al. 2006) after the burst. Attempts to observe the afterglow at radio wave bands resulted in upper limits (Soderberg 2005a, 2005b; Volvach & Pozanenko 2005). The optical afterglow was observed by Woźniak et al. (2005), Quimby et al. (2006), and Mason et al. (2006), resulting in coverage from a few seconds to ~4 days after the burst.

To construct the optical light curve, we have corrected the observed magnitudes for the standard Galactic extinction law given by Mathis (1990). The galactic extinction in the direction of GRB 050319 is estimated to be $E(B-V) = 0.011$ mag from the smoothed reddening map provided by Schlegel et al. (1998). The effective wavelength and normalization given by Bessell et al. (1998) were used to convert the magnitudes to fluxes in units of microjanskys.

Most of the GRB afterglow light curves are well characterized by a broken power law of the form $F = F_0[(t/t_b)^{\alpha_1 s} + (t/t_b)^{\alpha_2 s}]^{-1/s}$, where α_1 and α_2 are the afterglow flux decay indices before and after the break time (t_b), respectively; F_0 is the flux normalization; and s is the smoothening parameter that controls the sharpness of the break. Most known GRB afterglows have $\alpha_2 > \alpha_1$; i.e., the decay becomes steeper after the break. Interestingly, the optical afterglow light curve of GRB 050319 shows a steeper to flatter decay with a break at ~0.02 days. This behavior of light-curve decay is difficult to explain within the standard afterglow models. The X-ray and optical light curves also show some variability superimposed on the power-law decay. The X-ray light curve shows a break near ~0.3 days. We quantify the various characteristics of the afterglow light curves as summarized below.

1. The X-ray afterglow of GRB 050319 shows a very rapid decay ~0.005 days (~384 s) after the GRB. The decay then flattens before steepening again at ~0.3 days. Cusumano et al. (2006) have broken down the afterglow into three separate temporal evolutionary stages in the X-ray band: $\alpha_{X1} = 5.53 \pm 0.67$ ($\Delta t < 384$ s), $\alpha_{X2} = 0.54 \pm 0.04$ (384 s $< \Delta t <$ 0.3 days), and $\alpha_{X3} = 1.14 \pm 0.2$ ($\Delta t > 0.3$ days).

2. The *B*-, *V*-, and *R*-band light curves also show a rapid decline during the early phase ($\Delta t < 0.02$ days) that flattens at later epochs. Thus, the afterglow can be separated into two separate temporal evolutionary stages in the *R* band: $\alpha_{R1} = 1.09 \pm 0.03$ ($\Delta t < 0.02$ days) and $\alpha_{R2} = 0.51 \pm 0.03$ (0.02 days $< \Delta t <$ 10.0 days).

And for *B*, *V*, and *I* bands, we measure following α: $\alpha_{B1} = 1.46 \pm 0.26$ ($\Delta t < 0.02$ days) and $\alpha_{B2} = 0.33 \pm 0.05$ (0.02 days $< \Delta t <$ 1 day); $\alpha_{V1} = 0.90 \pm 0.05$ ($\Delta t < 0.02$ days) and $\alpha_{V2} = 0.50 \pm 0.04$ (0.02 days $< \Delta t <$ 1 day); and $\alpha_{I2} = 0.59 \pm 0.13$ (0.02 days $< \Delta t <$ 1 day). The average decay index of the optical light curve is then 1.15 ± 0.27 at the early epoch and 0.48 ± 0.15 at the late epoch.

4. GRB 050319 AFTERGLOW: WIND OR HOMOGENEOUS DENSITY PROFILE?

The breaks seen in the X-ray light curve (at ~384 s and at ~0.3 days) are not accompanied by simultaneous breaks in optical wave bands. Similarly, the break seen in the optical band has no simultaneous counterpart in the X-ray light curve. Also, the sense of slope change, i.e., $\alpha_2 < \alpha_1$, as seen in optical wave band is contrary to the predictions of the fireball model (Sari et al. 1996, 1998), which expects $\alpha_1 < \alpha_2$.

We propose a different model that explains the afterglow of GRB 050319 as being due to the transition of the circumburst medium density profile, which, in turn, is interacting with the explosion-generated shock wave. We propose that the observed change from steep to flat decay of the optical afterglow of GRB 050319 at 0.02 days is due to the change in the density profile of the circumburst medium from a wind-modified medium ($\rho \propto r^{-2}$) to a constant density medium ($\rho =$ constant). The break in the light curve occurs when the shock front interacts with the boundary between the two density profiles. Below we describe and reproduce the various features of the GRB 050319 afterglow using this model of "wind–to–constant-density medium transition."

The early steep decay of X-ray afterglows ($\alpha \sim 3$–5), as seen in the case of GRB 050319, are now seen routinely in most of the GRBs (Nousek et al. 2006) and have become a canonical feature of the GRB X-ray afterglows. In the case of GRB 050319, Cusumano et al. (2006) conjecture that the early steep decay emission could be the low-energy tail of the GRB prompt emission. We exclude this early emission from the remainder of our discussion, and we will restrict ourselves to the X-ray light curve.

The radiation spectrum of the GRB afterglows exhibits a power-law spectrum characterized by three break frequencies: the self-absorption frequency ν_a, the peak frequency ν_m corresponding to the lower cutoff in the electron energy distribution [$n(\gamma) \propto \gamma^{-p}$, $\gamma > \gamma_m$], and the synchrotron cooling frequency ν_c. The flux F_m at ν_m provides the normalization of the spectrum (Sari et al. 1998).

The photon indices (Γ) of the afterglow and the electron energy distribution index p are related in any given spectral regime ($\Gamma - 1 = p/2$ if $\nu_c < \nu$, and $\Gamma - 1 = (p-1)/2$ if $\nu < \nu_c$). The corresponding temporal decay indices α would be $(3p-2)/4$ and $3(p-1)/4$, respectively, before the jet break and would equal p in both spectral regimes after the jet break, according to the standard fireball model for an afterglow expanding in a homogeneous interstellar medium (ISM). For the shock wave expanding into the wind density profile, the corresponding α would be $(3p-2)/4$ and $(3p-1)/4$, respectively, before the jet break and would equal p after the jet break.

In the present case, the observed values of the photon index ($\Gamma = 1.69 \pm 0.06$) and the temporal decay index ($\alpha_X = 0.54 \pm 0.04$) of the X-ray afterglow are consistent with the spectral regime $\nu_X > \nu_c$ and $p = 1.5$. The observed decay indices of the optical light curve are also consistent with the inferred value of p, the spectral regime $\nu_{opt} < \nu_c$, and the transition from wind to constant density at 0.02 days. As discussed above, the expected temporal decay index of the X-ray afterglow, $\alpha_X = (3p-2)/4$, is the same for wind and homogeneous ISM density profiles. The absence of

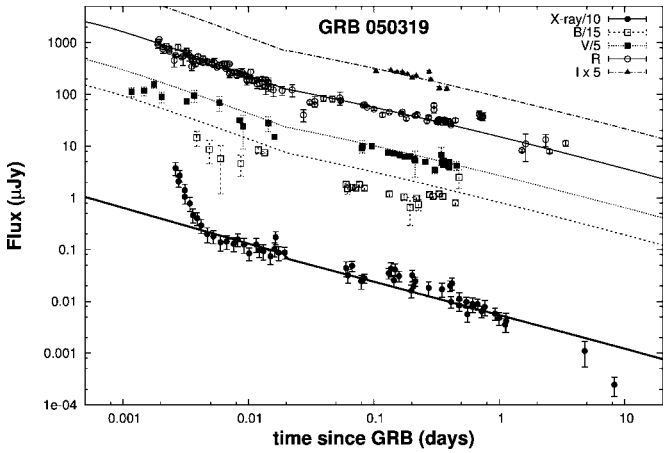

FIG. 1.—Afterglow light curves of GRB 050319. The solid lines represent a model in which the expanding fireball encounters the transition in density profile from the wind to constant density medium at 0.02 days. The best-fit spectral parameters of this model are listed in Table 2

a break in the X-ray afterglow light curve simultaneous with the optical break makes the multiband afterglow features consistent with the proposed transition of the circumburst medium density profile from wind to constant density. In Figure 1, we compare the predictions of our model of the transition from wind to constant density of the circumburst density profile with multiband observations of GRB 050319 afterglow. A detailed list of the best-fit spectral parameters can be found in Table 2. The observed *B*-band light curve is systematically lower than that predicted by the model, and this could be due to the Lyα absorption at $z = 3.24$ appearing in the observer's *B* band as suggested by Huang et al. (2007). The steepening of the X-ray light curve at $\Delta t \sim 0.3$ days could be due to a jet break (Cusumano et al. 2006), but unfortunately the variability in the *R*-band light curve and the insufficient sampling of the data in the *B* and *V* bands after ~1 day make it difficult to verify the achromaticity of the break.

Given the above model spectral parameters, we find that the broadband behavior of the afterglow is very well explained. However, we are restricting ourselves to the overall behavior of the afterglow, and hence we do not attempt to reproduce in our model the variations seen in the optical light curve. The reason for these variations could be the density inhomogeneities in the circumburst medium.

4.1. *Physical Parameters*

Four spectral parameters (ν_a, ν_m, ν_c, and $F_{\rm peak}$) are related to four physical parameters, viz., n (no density of the constant density circumburst medium) or A_* [defined as $\rho(r) = 5 \times 10^{11} A_* r^{-2}$ for wind density medium], E (total energy content of the fireball), and the energy fraction in relativistic electrons ϵ_e and that in the magnetic field ϵ_B. The typical value of the self-absorption frequency ν_a lies in radio-millimeter waves and hence is best estimated only if the afterglow is well observed in these bands. Unfortunately, the afterglow of GRB 050319 was never detected at the radio band (Soderberg 2005a, 2005b; Volvach & Pozanenko 2005). Therefore, we expressed the remaining three spectral parameters, known separately from parts of the light curves corresponding to the wind and the constant density circumburst medium, in terms of A_* and n, respectively. Equating the kinetic energies estimated from two density profiles, i.e., $E^K_{\rm wind} = E^K_{\rm ISM}$, we obtain a relation between A_* and n: $A_* = 5.097 \times 10^{-3} n^{2/5}$. For a typical range of values of n (1–100), estimated A_* ranges from 5.097×10^{-3} to 0.032, which results in the range of $E^K_{\rm iso}$ from 1.3×10^{54} to 5.3×10^{53} ergs. All the estimated physical parameters are listed in Table 3.

TABLE 2

THE BEST-FIT SPECTRAL PARAMETERS FOR WIND (<0.02 days) AND CONSTANT DENSITY (>0.02 days) PROFILE

Parameter	Wind Density Medium	Constant Density Medium
ν_m (Hz)	$1.6^{+0.9}_{-0.7} \times 10^{13}$	$1.0^{+0.35}_{-0.5} \times 10^{12}$
ν_c (Hz)	$1.1^{+3.7}_{-0.4} \times 10^{15}$	$2.1^{+0.6}_{-0.8} \times 10^{15}$
$F_{\rm peak}$ (μJy)	2370 ± 355	1810^{+260}_{-170}
p	1.59 ± 0.06	1.52 ± 0.02
χ^2(dof)	1.4(161)	

NOTE.—All the parameters are fitted at 0.003 days after the burst.

5. DISCUSSION

5.1. *Signature of Wind Reverse Shock?*

The morphology and evolution of the wind bubbles have been studied by Castor et al. (1975) and Weaver et al. (1977). A reverse shock forms at the surface, where the stellar wind meets the surrounding ISM, and it then propagates into the wind. The free wind (upstream of the reverse shock) has a density profile $\rho \propto r^{-2}$, and the shocked wind (downstream of the reverse shock) has a constant density profile. The effects of such a density transition on the afterglow of a GRB has been studied by Pe'er & Wijers (2006). It could be this transition of the density profile that we are observing at 0.02 days in the present case of GRB 050319. From the observations of long GRB afterglows, it has been inferred that most of the GRBs occur in the constant density environment and that the absence of wind signatures in the GRB afterglow was surprising. The various ways that can bring the wind reverse shock closer to the exploding star have recently been proposed to resolve this mystery surrounding the absence of winds (van Marle et al. 2006; Eldridge 2007). In the case of GRB 050319, for a range of assumed values of $n = 1$–100, we estimate the radius of the reverse shock to be $R_{\rm SW} \sim 0.5$–0.1 pc, comparable to the values obtained by Eldridge (2006). The constraint $\epsilon_B < 1$ puts a lower bound on density: $n > 0.03$.

5.2. *Implications for the Models of GRB Progenitors*

Our interpretation of the afterglow of GRB 050319 as being due to the transition from wind to constant density supports the collapsar model of GRBs. The detection of similar transitions in other afterglows has eluded us so far, perhaps because of the smaller size of the wind bubbles and the resultant early transition times. The present detection was made possible chiefly because of the quick follow-up abilities of the robotic telescopes RAPTOR (Woźniak et al. 2005) and ROTSE-III (Quimby et al. 2006) coupled with those of *Swift* XRT (Cusumano et al. 2006) and UVOT (Mason et al. 2006). Time

TABLE 3

PHYSICAL PARAMETERS ESTIMATED USING THE BEST-FIT SPECTRAL PARAMETERS MENTIONED IN TABLE 2

	$n = 1$; $A_* = 5.097 \times 10^{-3}$		$n = 100$; $A_* = 0.032$	
PARAMETER	Wind	ISM	Wind	ISM
$E^{\rm iso}_{54}$	1.3	1.3	0.53	0.53
ϵ_e	4.4×10^{-3}	2.2×10^{-3}	1.1×10^{-2}	5.4×10^{-3}
ϵ_B	0.14	1.2×10^{-3}	0.01	$\sim 10^{-4}$

dilation due to cosmological redshift delays the occurrence of the transition in the observer's frame of reference and makes it favorable to detect such a transition in distant GRBs. The robotic telescopes are now routinely detecting GRB afterglows as early as a few minutes after the burst, and with careful analysis of multiband observations of distant GRBs it should be possible to detect more examples of a similar transition. For example, a probable detection of a similar density transition, although not in the same wave band, has been reported by Gendre et al. (2007) in the case of GRB 050904 ($z \sim 6.3$), where the transition time is assumed to be ~1700 s (~0.02 days) after the burst, similar to that for the GRB 050319 afterglow in the present case.

6. SUMMARY

We have modeled the multiband afterglow of GRB 050319, using our own optical observations and other observations available in the literature, as being due to the interaction of the relativistic blast wave with circumburst medium, which shows a transition of the density profile from wind to constant density. Our conclusions can be summarized as follows:

1. We present *BVRI*-band observations of the GRB 050319 afterglow.

2. We show that the unusual break in the light curves of the optical afterglow at 0.02 days can be explained as being due to the transition of the circumburst density profile from wind to constant density. The observed X-ray afterglow light curve without a simultaneous break is consistent with this interpretation. The overall afterglow can be explained by using a relatively low value of the electron energy distribution index p that is also consistent with the X-ray spectral photon index.

3. The transition of the density profile could be due to the wind reverse shock propagating into the stellar wind driven by the progenitor of GRB 050319. We estimate the radius of the wind reverse shock to be $R_{\rm SW} \sim 0.5$–0.1 pc for assumed values of $n \sim 1$–100 cm^{-3}.

We are thankful to D. Bhattacharya for his critical comments and detailed discussions throughout this work and to Ram Sagar for his support during the observations. We are thankful to the anonymous referee for his/her constructive comments that have improved the Letter significantly.

REFERENCES

Bessell, M. S., Castelli, F., & Plez, B. 1998, A&A, 333, 231
Castor, J., McCray, R., & Weaver, R. 1975, ApJ, 200, L107
Chevalier, R. A., & Li, Z.-Y. 2000, ApJ, 536, 195
Cusumano, G., et al. 2006, ApJ, 639, 316
Eldridge, J. J. 2006, preprint (astro-ph/0610413)
———. 2007, MNRAS, 377, L29
Fynbo, J. P. U., Hjorth, J., Jensen, B. L., Jakobsson, P. Moller, P., & Näränen, J. 2005, GCN Circ. 3136, http://gcn.gsfc.nasa.gov/gcn3/3136.gcn3
Gendre, B., Galli, A., Corsi, A., Klotz, A., Piro, L., Stratta, G., Boër, M., & Damerdji, Y. 2007, A&A, 462, 565
Henden, A. 2005, GCN Circ. 3454, http://gcn.gsfc.nasa.gov/gcn3/3454.gcn3
Huang, K. Y., et al. 2007, ApJ, 654, L25
Krimm, H., et al. 2005a, GCN Circ. 3117, http://gcn.gsfc.nasa.gov/gcn3/317.gcn3
———. 2005b, GCN Circ. 3119, http://gcn.gsfc.nasa.gov/gcn3/3119.gcn3
Mason, K. O., et al. 2006, ApJ, 639, 311
Mathis, J. S. 1990, ARA&A, 28, 37
Misra, K., Bhattacharya, D., Sahu, D. K., Sagar, R., Anupama, G. C., Castro-Tirado, A. J., Guziy, S. S., & Bhatt, B. C. 2007, A&A, 464, 903
Nousek, J. A., et al. 2006, ApJ, 642, 389
Pe'er, A., & Wijers, R. A. M. J. 2006, ApJ, 643, 1036
Quimby, R. M., et al. 2006, ApJ, 640, 402
Rykoff, E., Schaefer, B., & Quimby, R. 2005, GCN Circ. 3116, http://gcn.gsfc.nasa.gov/gcn3/3116.gcn3
Sari, R., Narayan, R., & Piran, T. 1996, ApJ, 473, 204
Sari, R., Piran, T., & Narayan, R. 1998, ApJ, 497, L17
Schlegel, D. J., Finkbeiner, D. P., & Davis, M. 1998, ApJ, 500, 525
Soderberg, A. M. 2005a, GCN Circ. 3127, http://gcn.gsfc.nasa.gov/gcn3/3127.gcn3
———. 2005b, GCN Circ. 3132, http://gcn.gsfc.nasa.gov/gcn3/3132.gcn3
Stanek, K. Z., et al. 2003, ApJ, 591, L17
van Marle, A. J., Langer, N., Achterberg, A., & García-Segura, G. 2006, A&A, 460, 105
Volvach, A., & Pozanenko, A. 2005, GCN Circ. 3153, http://gcn.gsfc.nasa.gov/gcn3/3153.gcn3
Weaver, R., McCray, R., Castor, J., Shapiro, P., & Moore, R. 1977, ApJ, 218, 377
Wijers, R. A. M. J., & Galama, T. J. 1999, ApJ, 523, 177
Woźniak, P. R., Vestrand, W. T., Wren, J. A., White, R. R., Evans, S. M., & Casperson, D. 2005, ApJ, 627, L13